

Prostate Cancer Microvessels: A Novel Method for Three-Dimensional Reconstruction and Analysis

Paul A. Kay,^{1,2} Richard A. Robb,¹ and David G. Bostwick^{2*}

¹*Department of Physiology and Biophysics, Mayo Clinic, Rochester, Minnesota*

²*Department of Pathology, Mayo Clinic, Rochester, Minnesota*

BACKGROUND. Studies of prostate cancer microvessels to date have relied on routine two-dimensional images from histologic tissue sections, and there have been no previous reports of three-dimensional (3D) reconstruction and analysis of prostatic microvessels in benign or malignant specimens. Knowledge about the 3D architecture of microvessels would be useful for determining the utility and limitations of two-dimensional (2D) measures, as well as for determining the usefulness of 3D measures to predict pathologic stage and patient outcome in prostate cancer. However, the ability to study microvessels in 3D must first be demonstrated.

METHODS. We developed a novel method to visualize and analyze prostate microvessels in three dimensions from serially-sectioned prostate specimens, including tissue preparation, reconstruction of serial histologic sections into 3D volumes, extraction of vessels from this data set, and calculation of geometric characteristics. Eleven regions of benign and cancer tissue were studied and compared in an effort to validate our methodology.

RESULTS. Microvessels and glandular elements from benign and malignant tissue were visualized together in three dimensions. In the 3D visualizations, microvessels associated with cancer were seen to have more arbitrary pathways, increased tortuosity, and a more casual relationship with glandular elements than microvessels associated with benign tissue. A quantitative measure, the volume length density, discriminated between benign tissue and cancer better than simple microvessel density in this exploratory study.

CONCLUSIONS. Microvessels in prostate cancer have a more homogeneous distribution and greater tortuosity than those in benign tissue. Volume length density of microvessels shows promise as a 3D marker in prostate cancer. *Prostate 37:270–277, 1998.*

© 1998 Wiley-Liss, Inc.

KEY WORDS: prostate cancer; visualization; microvessels; angiogenesis; image processing

INTRODUCTION

Microvessel density is a useful predictive factor for pathologic staging of prostate cancer [1–3], and may be useful for determining patient outcome. Knowledge about the spatial and functional relationship of microvessels in benign tissue and prostate cancer is limited. Two-dimensional topographic studies of microvessels in prostate cancer have shown that microvessel density tends to be greater at the center of the cancer compared to the periphery, but the variance is modest [4]. Studies of the area of maximal density, termed the “hot spot,” have suggested that sampling

variation may lead to differences in microvessel density measured from biopsy specimens [3], but this has been refuted empirically [5]. We hypothesized that an understanding of the three-dimensional (3D) characteristics and patterns of microvessels in benign and malignant prostate tissue may indicate new 3D predictive measures of pathologic stage and patient outcome. The 3D spatial variations in microvessel den-

*Correspondence to: Dr. David G. Bostwick, Division of Anatomic Pathology, Mayo Clinic, 200 First St. SW, Rochester, MN 55905.

Received 19 January 1998; Accepted 22 May 1998

ties could also eventually be studied to find the degree of variation within benign and malignant prostate tissue and reveal whether needle biopsy provides a precise and representative sample of the tissue.

Three-dimensional reconstruction is the process of aligning serial histologic sections into a coherent three-dimensional volume. This method is widely used to study a variety of histologic tissues, but is tedious and labor-intensive [6–8]. The most popular approach involves manual registration of consecutive images of histologic sections, which are acquired from a video mixer at the time of evaluation [9]. Such user-operated approaches are time-consuming and subject to bias due to user expectations of constant section-to-section shape relationships [10]. Computer-based semiautomatic methods eliminate some of these reconstruction errors, but are generally slow, with processing rates of about 10 sections per hour [10]. The large number of sections required for accurate 3D reconstruction of prostate cancer microvessels demands a fast and automated method. Surface matching produces fast and accurate alignment of images [11], allowing registration of dissimilar serial sections. However, methods for surface matching of histologic serial sections and the resulting algorithms have not been developed and validated for prostate cancer.

Microvessels tend to vary in direction and orientation from section to section, a finding referred to as “anisotropism.” Anisotropic structures do not lend themselves to 3D reconstruction from two-dimensional sections [10]. The most common applications of 3D reconstructions have been with neuron cell bodies [10] and embryologic structures [12], which vary slightly from section to section. To accurately analyze microvessels, the method must be able to align anisotropic structures.

In this report, we present a novel method for 3D reconstruction, visualization, and analysis of microvessels in prostatic adenocarcinoma [13]. Analysis of 11 separate tissue foci from one patient demonstrated the potential of this process for the characterization of microvessel patterns in human cancers. We developed an accurate and rapid method for 3D reconstruction of the architecture of microvessels to facilitate quantitative study of their characteristics and patterns.

MATERIALS AND METHODS

We analyzed and visualized the 3D structure of microvessels from two-dimensional serial sections with the following steps: 1) preliminary phantom studies; 2) tissue preparations to optimize subsequent segmentation of microvessels and alignment of two-dimensional serial sections; 3) digital acquisition of

two-dimensional images from histologic slides; 4) segmentation of microvessels; 5) alignment of consecutive sections based on two-dimensional matching of spatial features (surface matching); and 6) visualization and analysis of 3D patterns.

Phantom Studies

To test the ability to accurately align and measure data from vessel-like structures, we constructed a phantom. The phantom was constructed from glass rods by the Mayo Clinic glass-blowing facility to simulate actual blood vessels. The goal was to obtain cross-sectional images from the phantoms which simulated the sectioning process. To produce these cross-sectional images, the phantom was scanned on a high-resolution spiral CT scanner. Once the images were scanned, they were resized to obtain pixel dimensions similar to those of vessels digitized from histologic sections. The result was an anisotropic vessel bed that could be arbitrarily misaligned to allow testing of our realignment algorithm and measuring process.

Tissue Preparation

Radical prostatectomy specimens with cancer were handled by whole-mount sectioning, as previously reported [14]. Each prostate was sliced at 4–5-mm intervals to create blocks of similar thickness, as per routine. Blocks were chosen for study which contained foci of cancer less than 3 mm in greatest dimension to ensure complete inclusion of the cancer and its margins. To ensure uniform section thickness, microtomes in our laboratory are regularly inspected and calibrated as part of our quality control system in surgical pathology. All sections from the chosen blocks were prepared and mounted routinely. Damaged sections that could not be mounted were recorded to account for their effect on the alignment and analysis of the microvessels. The small number of missing sections was not found to be detrimental to the overall process.

Serial histologic sections were differentially stained with antibodies to factor VIII-related antigen using the avidin-biotin-complex method. The chromagen used to highlight vessels was 3'-amino-ethyl-carbazole (AEC), which produced a red reaction product. Light hematoxylin was used as counterstain, and provided little interference with the color contrast of the blood vessels. Standard controls were used to ensure proper staining.

Each block was sectioned completely through at a thickness of 4 μm . Three blocks from one patient were used, and a total of 11 separate foci was reconstructed, with a mean number of 87 sections. Six of the 11 reconstructed volumes contained cancer. The cancer vol-

umes were acquired from three separate foci of cancer. Grades varied from Gleason score 4–6.

Digital Acquisition of Slide Images

A slow-scan color CCD camera attached to a Leitz PLANO microscope was used to acquire digital images for 3D reconstruction. Magnification was $\times 200$, with a resolution of $1,024 \times 774$ pixels, and pixel resolution was $1.37 \mu\text{m}$ for a total field of view of 1.402×1.060 mm.

Color images were acquired which consisted of red, green, and blue spectral images. These three-color images were combined in the display to produce a single full-color image. Each of the three-color images may be referred to as a “band” of information. Each band contained different information that was submitted to multispectral analysis [15] to classify the images into groups of pixels which represented desired structures, such as vessels and “nonvessels.”

Segmentation of Vessels

In multispectral analysis, the three-color bands were separated, and the pixel values of each were plotted as a histogram, sometimes referred to as “feature space” [15]. The value of a pixel in one band was compared to the value in another band, and tissues of different colors were located in different regions of the histogram plot. Using the Analyze™ multispectral tool, small sample regions of different objects could be specified, such as the vessels and background tissue. Classification algorithms separated the images into different characteristic classes according to the sample regions chosen. These algorithms assigned each pixel in an image to different objects, using the sample pixels as input. To evaluate the quality of the segmentation, sample images were segmented with various multispectral algorithms and compared to the actual specimens. We employed the K-nearest neighbor algorithm [15], which provided the best vessel segmentation and minimized segmentation errors. Prior to classification, the images were filtered using anisotropic diffusion [15] to reduce background noise while preserving edges. It was found that the glandular lumens could be segmented with a simple thresholding technique.

After final segmentation, the classified images were manually viewed and edited to correct obvious errors, which occurred in approximately 5% of sections. The segmented vessels were occasionally fragmented, and two-dimensional mathematical morphology [15] was performed on the segmented vessels to close small holes in the borders of vessels and to join fragmented areas.

3D Reconstruction

We undertook 3D reconstruction of the sequential digitized slices, using a combination of image-processing filters and an image registration algorithm in Analyze™. The method of registering sequential two-dimensional images included four steps: 1) feature images used to match consecutive sections were created using a Sobel edge filter in Analyze™, followed by simple thresholding, producing an enhanced edge image; 2) feature images were processed using mathematical morphology and connected component analysis [15] to eliminate noise and small structures, retaining only the large prominent features that could be located consistently from slice to slice; 3) extracted features were serially matched using a chamfer-distance surface matching algorithm [11] found in Analyze™; and 4) the transformation matrix from the matching process was used to transform the original image to bring it into alignment.

The first iteration of matching brought the images to general alignment. A second iteration was performed to closely approximate the vessels in the 3D reconstruction. In this iteration, the same four-step algorithm outlined above was used, but the feature images used were the segmented vessels. The surface matching algorithm was constrained, in this case, to look for matches in close proximity to the matches from the first iteration to speed up the process.

Verification of Alignment Accuracy

The accuracy of alignment was judged qualitatively because the true alignment was unknown due to the sectioning process. We used two common methods [10] to test the accuracy of alignment. In the first, we panned through each volume and successively removed the top layer, a viewing procedure similar to use of a movie loop which allows the user to visually detect any misaligned sections and record the level of misalignment. Misalignments were detected using this technique, and manually corrected. The second method, volume rendering of the objects, consisted of visual evaluation of the 3D reconstructions. The volumes were visualized using volume renderings of the reconstructed objects. The quality of the section-to-section alignment can be determined by the smoothness of the surfaces portrayed in volume rendering.

Analysis of 3D Characteristics and Patterns

Using the segmented microvessels, the volume percent of microvessels in the total sample volumes was calculated and compared to other measures. For benign tissue, the volume of the entire block was used,

and, in the cancer blocks, only cancer volume was used. The microvessel volume percentage was a true three-dimensional volumetric measure of the percent of volume of the microvessels. A size threshold of approximately 23 μm in diameter, as previously recommended [16], was used to count only those structures which were considered probable microvessels.

Microvessel density was calculated for each volume. Each cancer was defined by hand-tracing with Analyze™. The edge of the cancer in each section was manually traced as closely as possible to determine the volume by integration of the traced areas. In each two-dimensional (2D) section, the number of segmented vessels was counted. The microvessel density was then calculated as an average over the entire 3D stack of sections.

From the 3D microvessel data, we measured the tortuosity and total length of microvessels. To measure these patterns, the central pathway, or medial axis, of a vessel had to be determined. The medial axis of vessels was obtained by morphologic thinning [15]. In this process, a tube-like structure was reduced to a single voxel-thick connection of continuous points along the midline of the vessels. For connections of points, the path lengths, tortuosity, and other geometric characteristics were calculated.

A process was developed to acquire the medial axis of the vessels. The steps were: 1) introduction of blank slices to account for missing or damaged sections; 2) smoothing of vessels with a closing operation, using 3D mathematical morphology; 3) filling the vessel lumens, using a hole deletion algorithm; 4) resizing the volume to cubic dimensions of the slice thickness (the largest dimension); and 5) performing morphologic thinning on the resized cubic data sets to obtain the final vessel tree.

To measure tortuosity, the second derivative along each vessel pathway was calculated. The mean of the second derivative of all the medial axis points was obtained and used as a measure of vessel tortuosity. The second derivative of a path describes the rate of change in direction along that path. A second method used to measure tortuosity was to calculate the total length of vessels in a given volume, a measure that was referred to as “vessel length density” and that had units of vessel length per unit of volume.

Image Analysis Program

Software programs for processing and quantification of data were developed using the Tcl/Tk scripting language and AVW™ (Biomedical Imaging Resource, Mayo Foundation, Rochester, MN) programming library. Tcl/Tk is a graphics language for creating complex window interfaces quickly. The

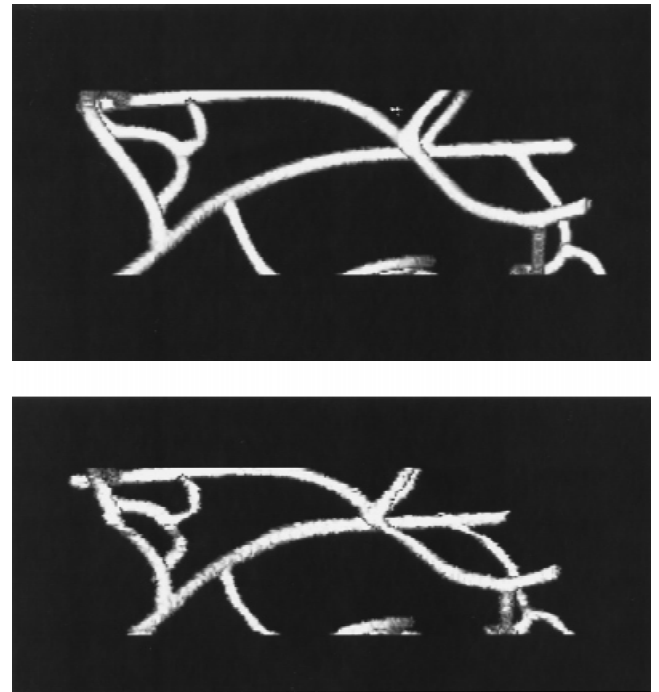


Fig. 1. Top: Volume rendering of the vessel-like phantom. Bottom: Same phantom, after misalignment and realignment, compares well to the original phantom.

AVW™ library of imaging processing functions [15] was bound to Tcl/Tk to allow quick construction of powerful image-processing functions. The tools needed to process, align, and analyze data for this research were embodied in two programs called “PathMatch” and “AnaPath.” These programs featured useful filtering functions, matching processes, and analysis features. Image-editing functions and multispectral analysis were performed by two programs in Analyze™.

RESULTS

Phantom Studies

The phantom used in this study was deliberately misaligned and realigned using the 3D reconstruction techniques which we had developed. By visually comparing the phantom before and after misalignment/realignment, it was apparent that we were able to adequately align the phantom (Fig. 1). The phantom was also used to validate the path length and tortuosity measures. Vessel lengths were manually measured from the phantoms, compared to computed measurements, and found to be consistent.

Alignment

Using the manual viewing method, 760 section-to-section matches were reviewed, and only 8 mis-

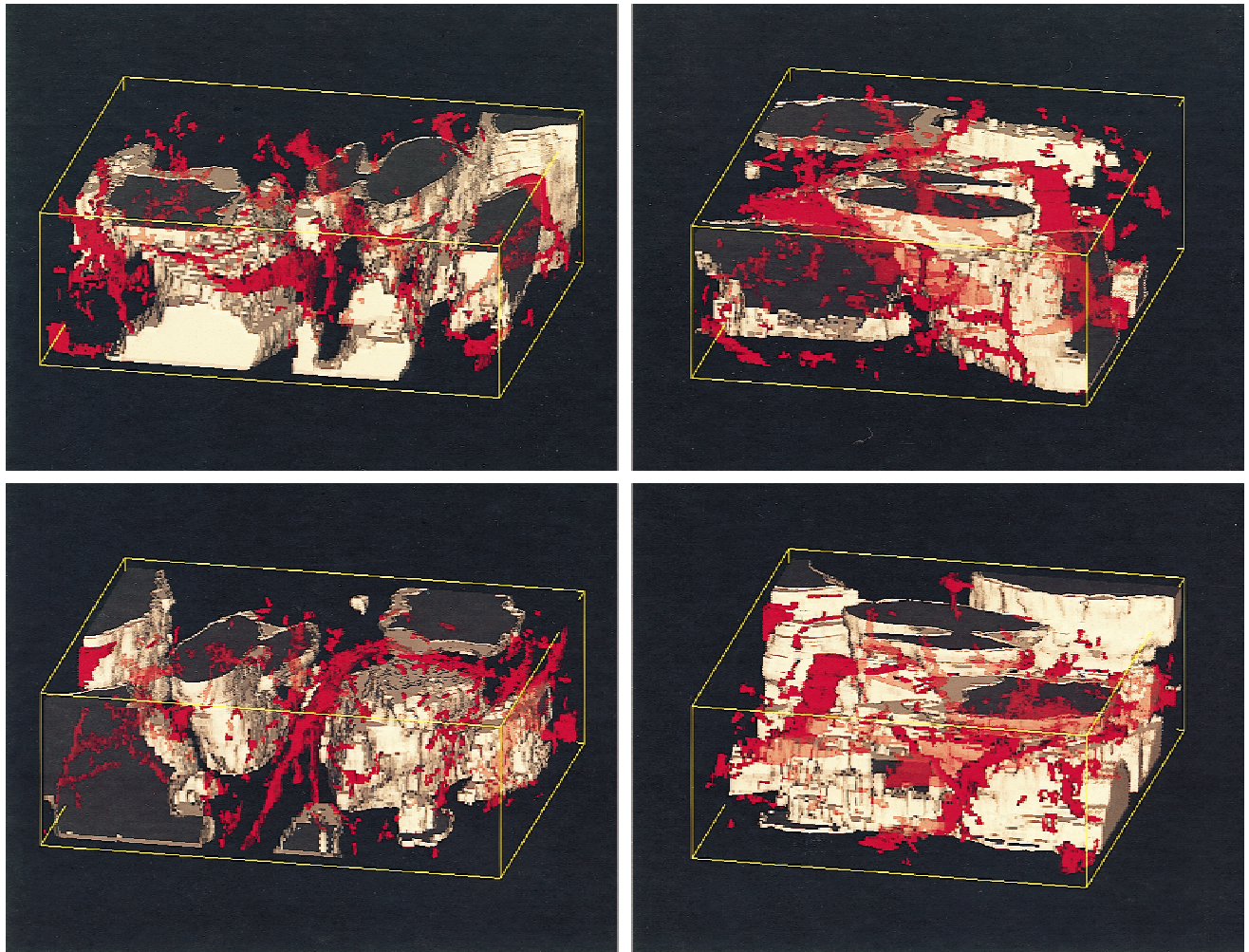


Fig. 2. Rotation sequence of volume-rendered benign tissue. Each image represents a 90° rotation of a 3D volume. The approximate size of the volume is $500 \times 500 \times 300 \mu\text{m}$. The gland lumens are tan and the vessels are red. The microvessels encircle the glands in a characteristic pattern.

matches were found that needed realignment. The matching process rarely failed when there were no missing or damaged sections; failures usually occurred at these gaps. The failure rate of matching over gaps was 9.2%, with an overall failure rate of 1.1%.

Volume renderings of the 11 regions were judged by the smoothness of the surfaces portrayed and were determined to be of acceptable quality (Figs. 2, 3). Vessels and glandular lumens appeared to be continuous and in good alignment in all cases. The renderings compared well with similar images of realigned objects appearing in recent reports [6,7,10,12].

In our sample, there was a marked visual difference in the volume renderings of the benign tissue and cancer. The lumens of the cancer acini were small and closely packed. The microvessels in this area were more numerous than in benign tissue, and appeared to be of uniform caliber, with extensive branching throughout. In benign tissue, gland lumens were

larger and the microvessels less numerous. In all cases, the vessels appeared to encircle lumens, although there appeared to be less order in the cancer samples.

Microvessel Density Counts

Microvessel densities calculated from this study are shown in Figure 4. The densities calculated compared well with those previously published [1–3]. The percentages of volume occupied by microvessel were calculated and are shown in Figure 5.

Length and Tortuosity

The results of the tortuosity measures based on the second derivative of the path are shown in Figure 6; those based on length density measures are shown in Figure 7. The tortuosity measures based on the second derivative did not show differences between mi-

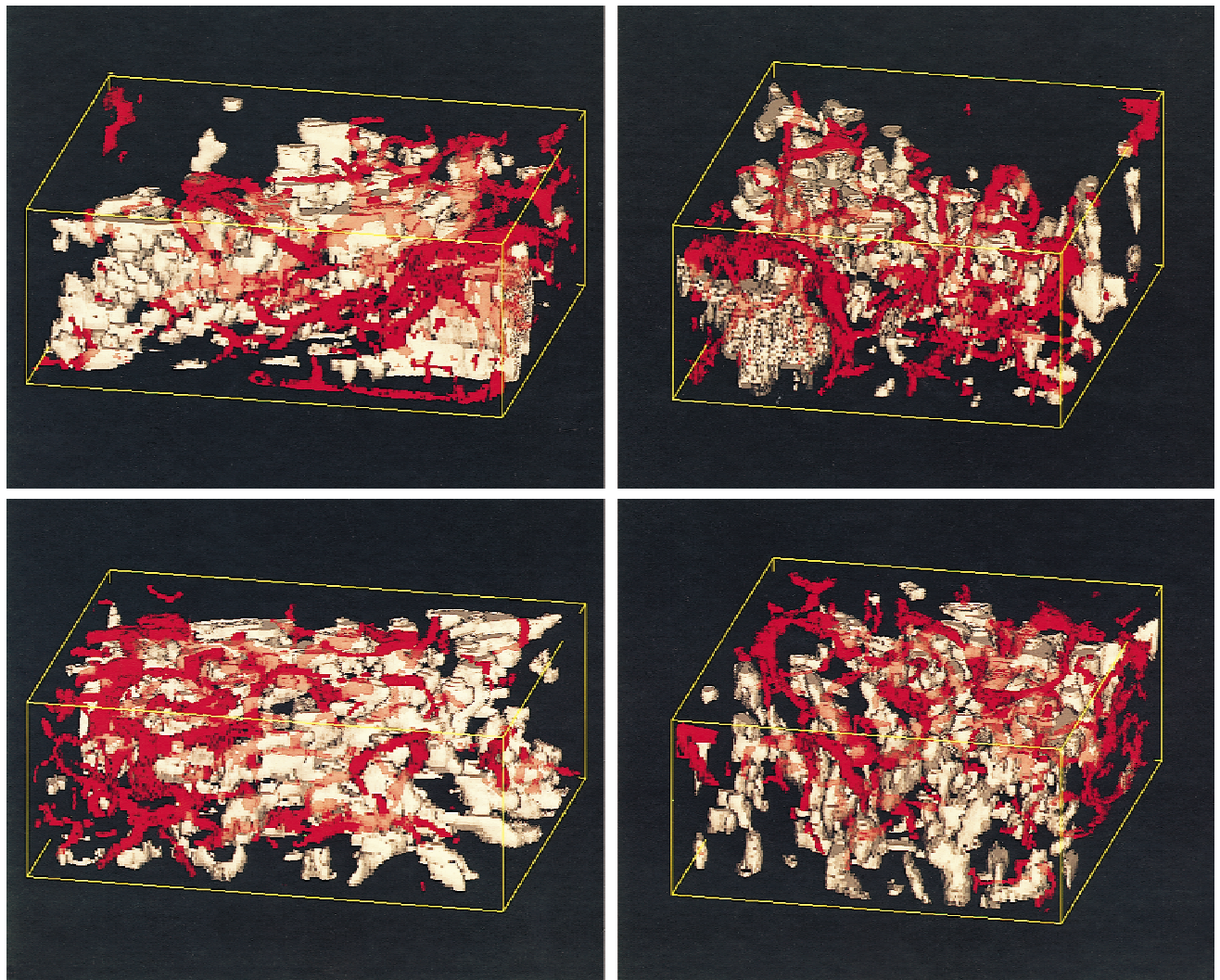


Fig. 3. Rotation sequence of volume-rendered cancer tissue. Each image represents a 90° rotation of the 3D volume. The approximate size of the volume is 500 × 500 × 300 μm. The gland lumens are tan and the vessels are red. The microvessels are seen to be more numerous, and they lack specific order of position.

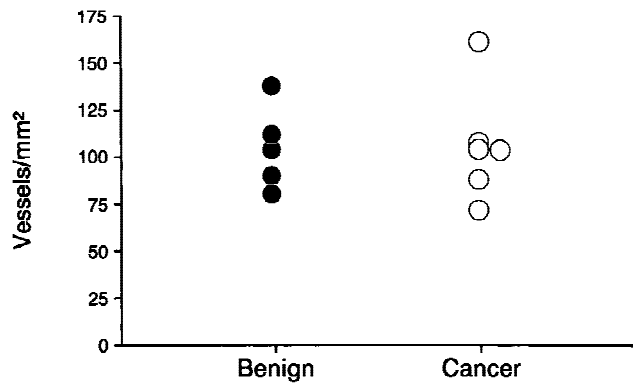


Fig. 4. Plot of microvessel density results (units: vessels/mm²). These results compare well to previously published results.

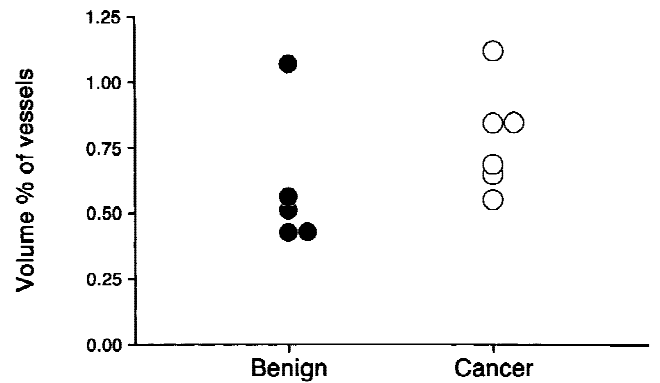


Fig. 5. This plot demonstrates the percentage of volume occupied by microvessels in tissue.

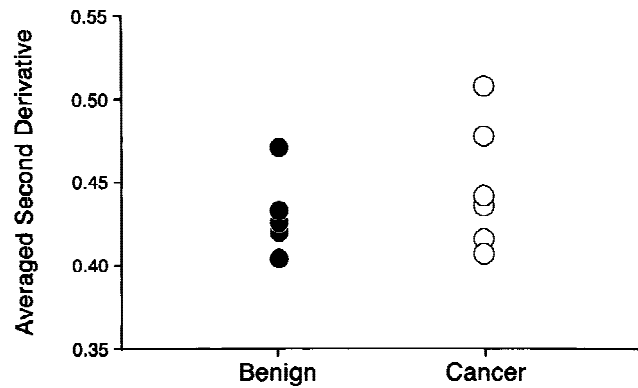


Fig. 6. The microvessel paths are described in this plot by the average second derivative along the path. The second derivative describes the rate of change along a path.

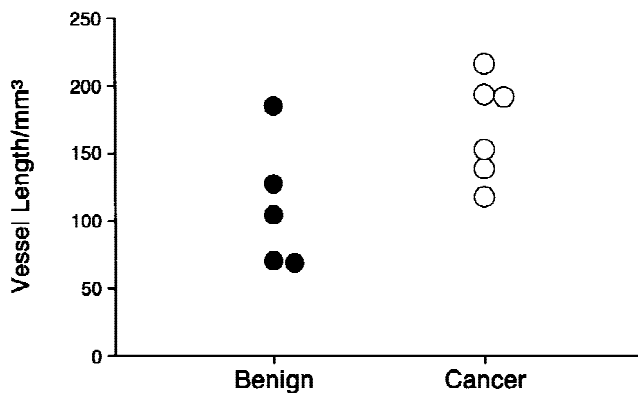


Fig. 7. Vessel length densities, which are defined as the total length of microvessels in a volume. Units of length density: mm length of vessels/mm³.

crovessels associated with benign and cancerous tissue. The length density measures appeared to separate the microvessel types more accurately.

DISCUSSION

In this study, we found that microvessels in prostate cancer were more homogeneously distributed than in benign tissue. In cancer, the microvessels were uniformly distributed among small acini, and appeared to be more tortuous, though this characteristic was difficult to quantitate. The microvessels in benign tissue were densely arranged around the glands. Among our quantitative measures, the best discriminator between microvessels in benign tissue and cancer was vessel length density, a relative measure of tortuosity. Other measures, such as the second derivative along the pathway and simple density counts, did not separate benign and cancer microvessels as well as vessel length density.

To create the 3D reconstruction, we developed a

novel method to align microvessels in serial histologic sections. The method was reproducible and robust, and has been applied to several tissues, including biliary ducts using varied acquisition techniques (data not shown). The technique can align approximately 150 slices/hr, which compares favorably to manual and other semiautomated methods of 3D reconstruction [6,10].

Though the goal of this research was to study microvessels, the glandular lumens of benign and malignant tissue were also visualized for the first time in 3D. This will allow future study of two separate tissue compartments, microvessels and glandular lumens, both separately and together.

Microvessel density, i.e., the number of microvessels in a given area, correlates with the pathologic stage of prostate cancer [1–3]. In Gleason scores of 5–7, microvessel density also correlates with cancer progression [17]. Our measures of microvessel density compare well to those in previous reports.

In 2D studies, the microvessels associated with prostate cancer were shorter, with more undulating vessel walls [18,19], than those observed in benign tissue. Optimized microvessel density, which is calculated from the microvessel density after discounting the glandular lumen space, correlated with pathologic stage when measured from a needle biopsy specimen [5]. When optimized microvessel density was added to the Gleason score and serum prostate-specific antigen (PSA) concentration, the predictive value of these measures increased. These results indicate that tissue from needle biopsies can be used to measure microvessel density clinically. However, the variance of microvessel density within cancer is well-known [4]. Attempting to measure the 3D microvessel bed with a needle biopsy may produce sampling variation errors.

The current study was limited by the small number of foci that were reconstructed. Due to the labor-intensive task of sectioning and digitally acquiring the data, this report validates our ability to study microvessels in three dimensions rather than definitively describing complex 3D measures. Methods are being developed to process a larger number of cases in a time-efficient manner. Three-dimensional studies may help validate the ability of a needle biopsy to adequately assess the nature of microvessels. Limited 3D views of prostate cancer microvessels may be quickly produced to reveal more information about the pathologic stage of the cancer involved than is available in current 2D images.

CONCLUSIONS

In conclusion, we developed a novel method for 3D reconstruction of microvessels. The vessels associated

with benign tissue and cancer were found to be different; the microvessels associated with cancer were seen to have more arbitrary pathways, increased tortuosity, and a more casual relationship with glandular elements than those in benign tissue. To our knowledge, this is the first 3D visualization and study of microvessels and glandular lumens in benign prostatic tissue and adenocarcinoma.

ACKNOWLEDGMENTS

We thank Drs. Robert Myers and Donald Cahill for their insight and helpful suggestions during this research. We also thank the staff of the Biomedical Imaging Resource at Mayo Clinic (Rochester, MN), and especially Jon Camp, for their expert help in image processing and programming.

REFERENCES

1. Bigler SA, Deering RE, Brawer MK: Comparison of microscopic vascularity in benign and malignant prostate tissue. *Hum Pathol* 1993;24:220-226.
2. Brawer MK, Deering RE, Brown M, Preston SD, Bigler SA: Predictors of pathologic stage in prostatic carcinoma. The role of neovascularity. *Cancer* 1994;73:678-687.
3. Weidner N, Carroll PR, Flax J, Blumenfeld W, Folkman J: Tumor angiogenesis correlates with metastasis in invasive prostate carcinoma. *Am J Pathol* 1993;143:401-409.
4. Siegal JA, Yu E, Brawer MK: Topography of neovascularity in human prostate carcinoma. *Cancer* 1995;75:2545-2551.
5. Bostwick DG, Wheeler TM, Blute M, Barrett DM, MacLennan GT, Sebo TJ, Scardino PT, Humphrey DA, Hudson MA, Fradet Y, Miller GJ, Crawford ED, Blumenstein BA, Mahran HE, Miles BJ: Optimized microvessel density analysis improves prediction of cancer stage from prostate needle biopsies. *Urology* 1996;48:47-57.
6. Salisbury JR, Whimster WF: Progress in computer generated three-dimensional reconstruction. *J Pathol* 1993;170:223-227.
7. Whimster WF: Problems of the third dimension. *Pathol Res Pract* 1989;185:594-597.
8. Merickel M: 3D reconstruction: The registration problem. *Comput Vis Graph Image Process* 1988;42:206-219.
9. Huijsmans DP, Lamers WH, Los JA, Strackee J: Toward computerized morphometric facilities: A review of 58 software packages for computer aided three dimensional reconstruction, quantification, and picture generation from parallel serial sections. *Anat Rec* 1986;216:449-470.
10. Rydmark M, Jansson T, Berthold CH, Gustavsson T: Computer assisted realignment of light micrograph images from consecutive sections of cat cerebral cortex. *J Microsc* 1992;165:29-47.
11. Jiang H, Robb RA, Holton KS: A new approach to 3-d registration of multimodality medical images by surface matching. *Proc Visual Biomed Comput* 1992;2:196-213.
12. Arraez-Aybar LA, Merida-Velasco JR, Rodriguez-Vazquez J, Jimenez-Collado J: A computerised technique for morphometry and 3D reconstruction of embryological structures. *Surg Radiol Anat* 1994;16:419-422.
13. Kay PA, Robb RA, Camp JJ, Bostwick DG: Three-dimensional visualization of microvessels in prostate cancer. *Proc Visual Biomed Comput* 1996;4:129-134.
14. Montironi R, Alexendar E, Bostwick DG: Prostate pathology case study seminar. *Virchows Arch* 1997;430:83-94.
15. Robb RA: "Three-Dimensional Biomedical Imaging: Principles and Practice." New York: VCH, 1995.
16. Wakui S, Furusato M, Itoh T, Sasaki H, Akiyama A, Kinoshita I, Asano K, Tokuda T, Aizawa S, Ushigome S: Tumour angiogenesis in prostatic carcinoma with and without bone marrow metastasis: A morphometric study. *J Pathol* 1992;168:257-262.
17. Silberman MA, Partin AW, Veltri RW, Epstein JI: Tumor angiogenesis correlates with progression after radical prostatectomy but not with pathologic stage in Gleason sum 5 to 7 adenocarcinoma of the prostate. *Cancer* 1997;79:772-779.
18. Montironi R, Diamanti L, Thompson D, Bartels HG, Bartels PH: Analysis of the capillary architecture in the precursors of prostate cancer: Recent findings and new concepts. *Eur Urol* 1996;30:191-200.
19. Barth PJ, Weingartner K, Kohler HH, Bittinger A: Assessment of the vascularization in prostate carcinoma: A morphometric investigation. *Hum Pathol* 1996;27:1306-1310.